Journal of Electroanalytical Chemistry 846 (2019) 113161

Contents lists available at ScienceDirect

Journal of Electroanalytical Chemistry

journal homepage: www.elsevier.com/locate/jelechem

The removal of phosphates using electrocoagulation with Al – Mg anodes

Adelaide Dura, Carmel B. Breslin*

Department of Chemistry, Maynooth University, Maynooth, Co. Kildare, Ireland

ARTICLE INFO

Keywords:
Electrocoagulation
Al-Mg anode
Phosphates
Adsorption
Coagulants

ABSTRACT

The removal of phosphates, to levels below the detection limit, was achieved over a 30 to 60 min period, depending on the initial phosphate concentration, with Al – Mg anodes in an electrocoagulation cell at 11.0 mA cm^{-2} with a surface area to volume ratio of 11.7 m^{-1}. The Al – Mg alloy performed well in low chloride concentrations of 4.2 mM NaCl and the complete removal of phosphates from two real water samples was achieved after a 15 – min period. The removal efficiency, although depending on the initial pH, appears to depend on the evolution of pH during electrocoagulation with more efficient removal at a final pH of 7.5. Using the Freundlich adsorption model, the adsorption capacity, k_F, was computed as 146 mg g^{-1}, corresponding to the adsorption of 146 mg of phosphate per gram of the aluminium – hydroxy coagulant. The efficient removal of the phosphates was attributed to the low corrosion potentials and the lack of a passive region observed using polarisation and cyclic polarisation experiments, which in turn facilitate dissolution of the anode.

1. Introduction

Phosphorus occurs naturally in water and wastewater mainly as inorganic phosphates, such as orthophosphates and polyphosphates [1]. However, the presence of excess phosphorus in the effluent discharged to natural water bodies has long been known to be associated with algal bloom and eutrophication, particularly if nitrates are also present. Because of these problems, phosphate removal using chemical precipitation and coagulation has been carried out for a number of years [2,3]. Recently, other physicochemical processes have been used to remove phosphate from wastewater as alternatives to the more traditional methods. These techniques include adsorption with various adsorbents, ion – exchange, electrodialysis, hybrid systems containing adsorption and membrane filtration and electrocoagulation [4–6].

In terms of a comparison between coagulation and electrocoagulation, it has been reported that electrocoagulation has a number of advantages. The energy required in the dissolution of the sacrificial anodes can be provided by green energy, such as solar panels [7]. Secondary pollution is minimised as no chemicals are added. Moreover, it produces low amounts of sludge and the flocs tend to be large, contain low amounts of bound water, are stable and therefore can be easily separated by filtration. The generation of gas bubbles, produced during electrolysis at the cathode, is considered another advantage as the bubbles can carry the lighter flocs to the top of the reactor where they can be more easily collected. It is not surprising that in recent years, there has been considerable interest in electrocoagulation and different pollutants have been removed [8–10]. Electrocoagulation is particularly suited to the removal of phosphates and these anions have been removed successfully using pure aluminium and iron anodes [10–14].

In electrocoagulation, sacrificial anodes are employed and these usually involve iron or aluminium. As the metals dissolve, cations, Al^{3+} or Fe^{2+}, are produced, while hydroxide ions and hydrogen gas are generated at the cathode in the cell. This leads to an increase in the OH^- concentration and an increase in the bulk solution pH. As a result, the cations are hydrolysed and this gives rise to the formation of various hydroxy – complexes, which favour the coagulation – flocculation process and removal of the pollutant [8]. The coagulation – flocculation process is complex and depends on the operating conditions used, the type and concentration of the pollutant and the type and concentration of the coagulant species. The coagulants depend on the concentration of the electrogenerated cations and this in turn is connected with the properties of the anode.

Although iron and aluminium are routinely employed, alloys may have positive effects in terms of removal efficiency and energy consumption. In a recent study, we showed that Al – Mg and Al – Zn – In alloys were more efficient than pure aluminium in the treatment of a synthetic wastewater [15]. This was attributed to the less passive behavior of the alloys and their ease of dissolution, compared to pure Al that forms a stable passive film. The formation of passive films or oxides, not only inhibits the dissolution of the anode, but gives rise to localised corrosion, such as pitting attack in the presence of chloride anions [16]. The breakdown or pitting potentials are well below the cell

* Corresponding author.
E-mail address: Carmel.Breslin@mu.ie (C.B. Breslin).

https://doi.org/10.1016/j.jelechem.2019.05.043
Received 8 January 2019; Received in revised form 16 May 2019; Accepted 16 May 2019
Available online 21 May 2019

potentials employed during electrocoagulation, indicating that any material prone to pitting attack will dissolve in a non−uniform manner. Furthermore, the passive film inhibits dissolution and restricts the charge−transfer reaction at the anode−solution interface and this leads to excessive consumption of electricity and reduces the energy efficiency of the process.

In this study, Al−Mg was used as an anode in an electrocoagulation cell for the removal of phosphates. To the best of our knowledge, this alloy has not been used previously in the removal of phosphates. Instead, aluminium anodes, typically at 99.0% to 99.9% purity have been employed, which contain various impurities, such as Cu, Si and Fe [17,18]. In our previous paper [15], a synthetic wastewater was employed containing an organic dye, zinc and phosphate ions, together with sulfates, chlorides, calcium and magnesium ions. A less complex solution where phosphate is the only pollutant, in a low 4.2 mM NaCl solution, is now considered, resulting in no competition between the pollutants during the removal of the phosphates. Using a combination of electrocoagulation experiments, adsorption studies and corrosion related measurements, the potential application of the Al−Mg as an anode in an electrocoagulation cell is evaluated. The Al−Mg anode was used to remove phosphates at different pH values, chloride ion concentrations and to remove phosphates from real wastewater samples.

2. Experimental method

All chemicals were supplied by Sigma−Aldrich®. Potassium dihydrogen phosphate, KH_2PO_4, was used as the source of phosphates. All solutions were prepared using distilled water and the pH was adjusted to the desired value. The phosphate concentrations were measured using the vanadomolybdo-phosphoric acid colorimetric method [19] at 470 nm using a Unicam Thermo Spectronic® UV 540 double−beam spectrometer. Following the electrocoagulation experiment, 5−mL samples were taken from the reactor and allowed to settle for 15 min. This solution was replaced with fresh aliquots to maintain a constant SA/V ratio and all computed concentrations were corrected for this dilution. Then, the supernatant was filtered with Whatman™ filter membranes (pore size 11 μm, followed by 0.45 μm). A 3.5 mL sample of this filtered solution was combined with an equal volume of the vanadate-molybdate reagent, allowed to sit for 10 min and then analysed for the presence of phosphate. Using this approach very good reproducibility was achieved with the difference in the measured absorbance being less than 0.003 for repeated measurements. The removal efficiency, η, was calculated using Eq. (1), where C_o is the initial concentration of the analyte and C_t is the concentration of the analyte at time t. The experiments were repeated at least three times and this is indicated by the n value shown in the figure captions. The limit of detection, DL, was obtained using the regression line of the calibration curve and Eq. (2), where y_B is the blank signal and s_B is the standard deviation of the blank. The detection limit was estimated as 0.15 mg L^{-1} phosphate.

$$\eta(\%) = \frac{C_o - C_t}{C_o} \times 100 \quad (1)$$

$$DL = y_B + 3s_B \quad (2)$$

The Al−Mg alloys were supplied by Goodfellow© with the following composition: 1.7–2.4% Mg, 0.5% Fe, 0.5–0.1% Mn, 0.4% Si, balance Al. The samples used in the electrocoagulation tests were cut to form sheets with dimensions of 4.0 cm × 6.0 cm. The sheets were abraded with water lubricated Buehler® silicon carbide paper (Grit P 320 to P 2500), washed with deionised water and dried in a stream of air. The electrocoagulation tests were carried out using a two−electrode cell with a steel cathode (AISI 310) in 4.2 mM NaCl at room temperature. The electrodes were positioned and held in the cell (300 cm^3 of solution) to give an immersed surface area of 35.1 cm^2 and a surface area to volume of solution ratio, SA/V, of 11.7 m^{-1}. The distance between the anode and the cathode was maintained at 1 cm to facilitate good solution mixing and to reduce Ohmic (IR) drops that were evident at higher distances. The solution was agitated and a constant current density of 11.0 mA cm^{-2} was applied to deliver a fixed amount of Al^{3+} to the solution phase. For comparison purposes, pure Al (99.9%) was employed as the anode in the electrocoagulation cell.

The electrochemical behaviour of the Al−Mg anode was studied using polarisation experiments with a Solartron 1287 potentiostat. These tests were carried out in a three−electrode cell with a saturated calomel electrode as the reference and a high surface area platinum wire as the counter electrode. The Al−Mg rod electrodes, employed as the working electrode, were prepared and set in a Teflon® holder with epoxy resin. Electrical contact was made using a copper wire, which was threaded to the base of the sample. The exposed electrode surface was abraded on a Buehler® MetaServ grinder polisher with water lubricated Buehler® SiC grinding papers to a 2500 grit finish. The electrodes were then sonicated in a Branson 1510 ultrasonic bath and polished with successively finer grades of Buehler® MetaDi monocrystalline diamond suspensions ranging from 30 to 1 μm on Buehler® polishing microcloths. Finally, the electrodes were rinsed with deionised water and ethanol, sonicated and dried in a stream of air. The electrodes were polarised from 300 mV below the corrosion potential, E_{corr}, at 1.0 mV s^{-1} following a 30−min immersion period. In cyclic polarisation measurements the potential was reversed and cycled in the opposite direction when the current reached 0.01 mA cm^{-2}. Electrochemical impedance spectroscopy measurements were performed with a Solartron 1287 potentiostat coupled with a 1255B frequency response analyser using a perturbation potential of 5 mV at the open−circuit potential. Optical micrographs were recorded using an Olympus® BX51M microscope at different magnifications in a dark−-field mode. The micrographs were collected with a CCD camera (Leica DFC 2280 digital camera) and Olympus® DP version 3.2 software.

The phosphate removal was fitted to adsorption isotherms. These experiments were performed by varying the initial concentration of phosphate from 2.0 to 150.0 mg L^{-1} in 4.2 mM NaCl, at a pH of 5.0 at 25 °C. The data were analysed using SigmaPlot™. A non−linear regression method based on the Levenberg−Marquardt algorithm was used to fit the experimental data with the adsorption equations and the goodness of fit was obtained using the adjusted R^2 values.

3. Results and discussion

3.1. Removal of phosphates

In Fig. 1, the normalised concentrations of phosphate, P_t/P_o, are plotted as a function of the electrocoagulation period in solutions containing 20, 60 and 150 mg L^{-1} of phosphate in a 4.2 mM NaCl solution adjusted to a pH of 5.0. In this analysis, P_t represents the concentration of phosphate at time, t = t min and P_o represents the initial concentration at time, t = 0 min. This relatively low concentration of chloride was used to reflect the typical concentrations of chloride found in wastewater samples, while the initial pH of 5.0 was used as it is generally accepted that slightly acidic pH values give more efficient removal. It is evident that the phosphate concentration is reduced to very low levels for all three concentrations following a 60−min period, where the efficiency was greater than 98% for all three solutions. However, it is also clear that the experiments performed at lower initial concentrations show higher removal efficiencies at shorter times. This is evident in Table 1, where the efficiencies are shown following a 10−min, 20−min and 60−min electrocoagulation period. For comparison purposes, similar data are presented for pure aluminium at initial phosphate concentrations of 20 and 60 mg L^{-1}, and while the removal of phosphates is readily achieved, the removal efficiency is somewhat lower than that observed with Al−Mg as the anode materials. The removal of phosphates can also be described by Eq. 3, where [P] is the concentration of phosphate, $[Al(OH)_n^{(3-n)}]$ is the

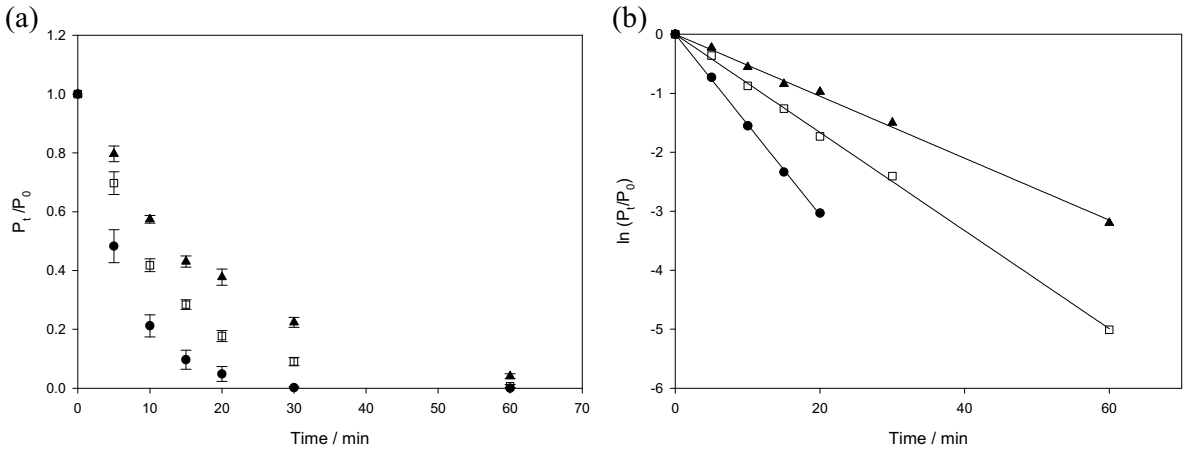

Fig. 1. Variation of (a) concentrations, P_t/P_o, of phosphate and (b) first−order kinetics plots in solutions containing P_o of ● 20 mg L^{-1}, □ 60 mg L^{-1} and ▲ 150 mg L^{-1} (n = 3).

Table 1
Removal efficiency (η) as a function of time and initial concentration of phosphate (P_o), at a pH of 5.0 in 4.2 mM NaCl.

Al-Mg			Pure Al
t/min	P_o/mg L^{-1}	η/%	η/%
10	20	79 ± 4	68 ± 3
	60	58 ± 2	41 ± 2
	150	43 ± 1	
20	20	95 ± 3	84 ± 4
	60	82 ± 2	70 ± 2
	150	62 ± 3	
60	20	100[a]	97 ± 2
	60	100[a]	95 ± 2
	150	96 ± 0.8	

[a] 100% indicates concentration is below detection limit.

concentration of the hydrolysis products of Al^{3+} ions, k is the rate constant, and x and y are the partial orders of the reaction. Assuming that the production and consumption rates of the hydrolysis products are equal, then Eq. (3) can be reduced to Eq. (4), where x is the order of the reaction.

$$\frac{d[P]}{dt} = -k\,[P]^x\,[Al(OH)_n^{3-n}]^y \quad (3)$$

$$\frac{d[P]}{dt} = -k_{obs}\,[P]^x \quad (4)$$

In this approximation the rate constant reflects the contribution of several reactions, involving both the coagulation and the flocculation phases. Typical plots where the logarithm of P_t/P_0 is shown as a function of time are presented in Fig. 1(b), assuming x is unity. The linear plots indicate that the rate of the reaction is governed by pseudo first−order kinetics during the early stages of removal. It is clearly evident that the rate constant, k_{obs}, decreases with increasing initial concentration of phosphate, with k_{obs} values varying from 0.1531 min^{-1} for 20 mg L^{-1}, 0.0832 min^{-1} for 60 mg L^{-1} to 0.0525 min^{-1} for 150 mg L^{-1} of phosphate. This decrease in removal efficiency with increasing initial concentrations has been reported for several pollutants [20,21] and is explained in terms of the ratio of coagulant, the aluminium hydroxycomplex species, to pollutant. When the ratio is low, corresponding to high initial phosphate concentrations, the rate of removal is slow. The influence of the applied current density is illustrated in Table 2, where the rate constants for the removal of phosphate are shown at current densities of 5 and 11 mA cm^{-2}. It is clearly evident that the phosphate is removed at a higher rate when the current density is maintained at 11 mA cm^{-2}. On the application of a higher current density, the cell potential increased giving a more significant energy consumption and therefore the current density was maintained at 11 mA cm^{-2}.

Table 2
Influence of the current density on the rate of removal of phosphate from a 4.2 mM NaCl solution.

P_o/mg L^{-1}	Current density 5 mA cm^{-2}		Current density 11 mA cm^{-2}	
	k_{obs}/min^{-1}	R^2	k_{obs}/min^{-1}	R^2
20	0.0877	0.995	0.1531	0.999
60	0.0487	0.994	0.0832	0.999
150	0.0274	0.995	0.0525	0.997

The influence of pH on the rate of phosphate removal was studied using a solution containing 85 mg L^{-1} of phosphate. The concentrations of phosphate remaining in solution as a function of the electrocoagulation period are displayed in Fig. 2(a). The maximum removal of phosphate is achieved at a pH of 3.2 with a residual phosphate concentration of 1.1 mg L^{-1} after a 30−min period. On increasing the initial pH, a gradual decrease in the amount of phosphate removed from the solution is observed. There is no general agreement on the optimal initial pH required to remove phosphates. According to Bektaş et al. [22] the optimal initial pH for phosphate removal is 5.0 to 6.0. A similar finding was reported by Vasudevan et al. [23], while İrdemez and co-workers [24] demonstrated that the highest efficiency was achieved at an initial pH of 3.0. These variations are probably connected to the manner in which the pH evolves during electrocoagulation. This relationship between the initial and final solution pH is illustrated in Fig. 2(b). When the initial pH is acidic, the final pH value shows a marked increase, from 3.2 to 7.1. On the other hand, solutions with initial pH values close to neutrality exhibit a more moderate rise. This increase in pH is normally attributed to the water reduction reaction at the cathode, Eq. (5), and this in turn will depend on the rate of the alloy dissolution reaction. The pH will influence the nature of the aluminium hydroxy species and this is shown in Fig. 3(a) which was obtained using the algorithm developed by Eriksson [25]. It is evident that the monomeric hydroxy−aluminium cations are stable at low pH, while increasing the pH to values close to 7.0 leads to the production of cationic aluminium hydroxy species, and the $Al(OH)_3$ precipitate. It is evident in Fig. 3(b) that the phosphate exists as anions, from about pH 3.0 to 14.0. Initially at a pH of 3.0, the Al^{3+} ions exist and while electrostatic interactions between Al^{3+} and the anionic $H_2PO_4^-$ are possible, these are unlikely to give rise to efficient removal of the phosphates. However, these acidic conditions will inhibit the formation

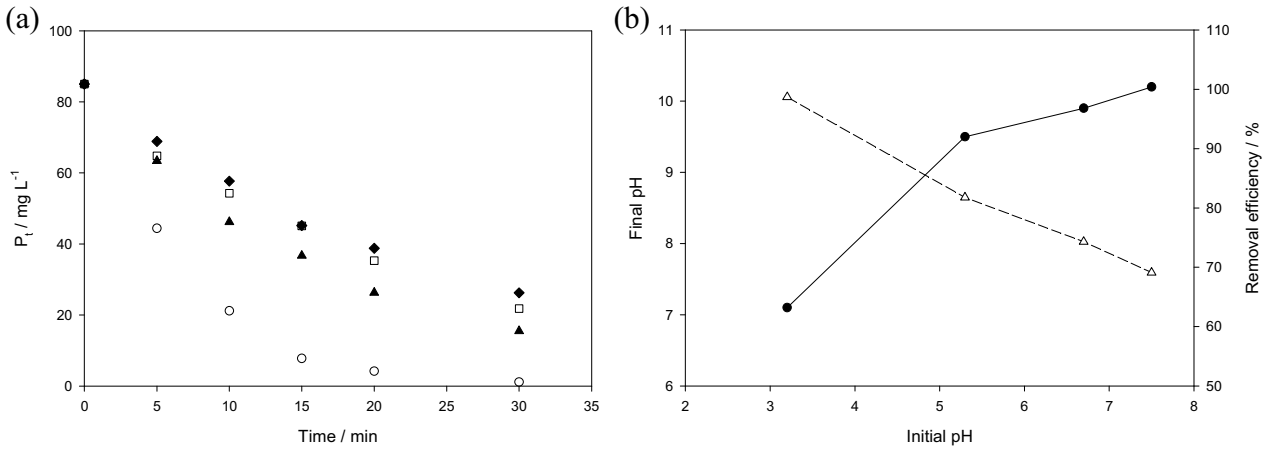

Fig. 2. (a) Variation of the residual phosphate concentration, P_t, plotted as a function of time in solutions containing 85 mg L^{-1} of phosphate at initial pH values of ○ 3.2, ▲ 5.3, □ 6.7 and ♦ 7.5. (b) Evolution of ● final pH and △ removal efficiency (calculated at t = 30 min) plotted as a function of the initial pH.

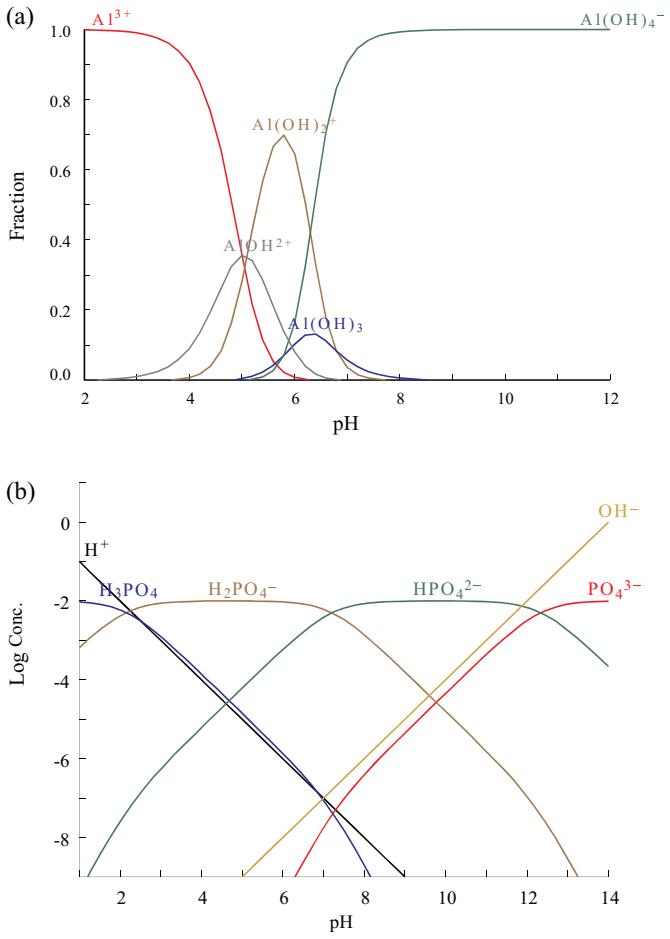

Fig. 3. Speciation diagrams of the hydrolysis products for (a) Al^{3+} and (b) phosphate ions at a concentration of 1.0 μM. The diagrams were realised using the algorithm developed by Eriksson [25].

of passive films at aluminium, as evident from the Pourbaix diagram of aluminium. As more Al^{3+} is electrogenerated, the pH changes rapidly due to the water reduction reaction at the cathode, Eq. (5), until the aluminium – hydroxy species are formed to give a buffering – type effect, with the removal of OH^- form the solution. Now electrostatic interactions are possible between the anionic phosphate and the cationic $Al(OH)_2^+$ and $AlOH^{2+}$, and indeed other hydrolysed aluminium hydroxy species, facilitating the efficient removal of phosphate. It has been shown that insoluble $AlPO_4$ is also formed [4]. As illustrated in Fig. 3, the formation of small amounts of insoluble $AlPO_4$ is possible at a pH in the vicinity of 6.0 to 7.0, where the Al^{3+} and PO_4^{3-} ions co – exist. While the concentrations are very low, once these ions are removed through the precipitation of $AlPO_4$, they will be restored as a new equilibrium position is established to give further precipitation of the insoluble $AlPO_4$. It appears that a final pH which is close to neutral conditions, where the aluminium hydroxy species and anionic phosphates exit at relatively high concentrations, and where $AlPO_4$ has a low solubility [4], provide the highest removal efficiency, as illustrated in Fig. 2(b).

$$2H_2O + 2e^- ? 2OH^- + H_2(g) \quad (5)$$

The effect of chloride concentration on electrocoagulation has been investigated in a number of studies [26,27] with some authors recommending that the solution contains at least 20% Cl^- ions to ensure normal operation [28]. In Fig. 4(a) the residual concentration of phosphate after 30 min in solutions containing various concentrations of NaCl and 85 mg L^{-1} phosphate is shown. A near 10 – fold increase in the NaCl concentration, from 4.2 to 44 mM, results in a slight increase in the removal efficiency from 85.2% to 88.8%. However, the chloride concentration has a marked effect on the potential adopted by the Al – Mg anode and consequently the energy consumption. The potential is shown as a function of the electrocoagulation period in Fig. 4(b), where it is clearly evident that the potential increases to more positive potentials with decreasing chloride concentrations and this increase is more significant at the lower chloride concentrations. Furthermore, while the anode potential is reasonably constant in the presence of higher chloride concentrations, it tends to increase further with increasing electrocoagulation times in the presence of lower chloride concentrations. In solutions containing 4.2 mM NaCl the average cell potential is 2.2 V vs. SCE, but then increases after about 1500 s to approximately 3.0 V vs SCE. This is probably related to passivation of the anode and as a result higher potentials are required to deliver the required current. As the chloride concentration is low and there is an increase in the pH of the solution during electrocoagulation, passivation of the anode is favoured, over its dissolution. At these potentials, concurrent reactions occur at the anode, such as the oxidation of water (E^o = 1.23 V vs. SHE) or the formation of chlorine – containing oxygen compounds [29]. Although these side reactions may help flotation or pollutant oxidation, they give rise to a lower current efficiency. The energy consumption, in terms of specific electrical energy consumption (SEEC), was computed using Eq. (6), where E_{cell} is the average cell voltage, J is the current, t is the electrocoagulation time, and V is the volume of the solution treated. The energy consumption was found to vary from 3.15 to 0.15 kWh m^{-3} as the chloride concentration was

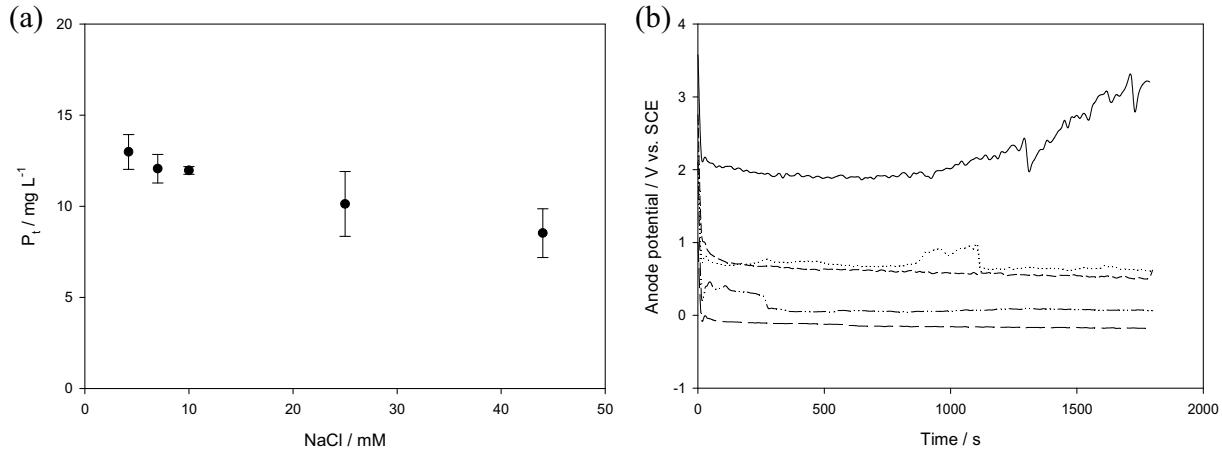

Fig. 4. (a) Residual phosphate concentration, P_t, after 30 min as a function of NaCl concentration (n = 3), (b) anode potential as a function of the chloride concentration —— 4.2 mM, · · · 7.0 mM, – – – 10.0 mM, – ·· – 25.0 mM, and —— —— 44.0 mM NaCl.

increased from 4.2 to 44 mM. These data illustrate the important role of the solution conductivity and the chloride concentration.

$$SEEC = \frac{E_{cell} Jt}{V} \tag{6}$$

3.2. Polarisation behavior of Al – Mg

The potentiodynamic polarisation curves recorded for Al – Mg in 0.017 M and 0.170 M NaCl solutions are compared in Fig. 5(a). These two concentrations were chosen as the 0.170 M NaCl solution is conducting with little resistance (no IR drop) in the electrochemical cell, while a 10 – fold decrease in the chloride concentration to give a 0.017 M NaCl solution is more representative of the typical chloride concentrations found in water or wastewater samples. The corrosion potential, E_{corr}, in 0.170 M NaCl is −0.664 V vs. SCE, compared to a value of −0.554 V vs. SCE in 0.017 M NaCl. The corrosion currents, j_{corr}, were computed using the Tafel equation, Eq. (7), where η represents the overpotential, E is the applied potential, j_{corr} is the corrosion current density, j is the measured current density and α is the transfer coefficient.

$$\eta = E - E_{corr} = \frac{2.303RT}{\alpha F} \log j_{corr} - \frac{2.303RT}{\alpha F} \log j \tag{7}$$

The corrosion current density j_{corr}, was computed as 1.20×10^{-6} A cm^{-2} for both chloride concentrations, indicating little influence of chloride concentrations between 0.017 M and 0.170 M. The current density increases sharply at potentials higher than E_{corr}. Consequently, the electrode exhibits no clear passive region and in electrocoagulation applications this feature would be advantageous for the energy supply to the system. The breakdown potentials, E_{br}, were taken at a reasonably high current density of 0.01 mA cm^{-2}, and in 0.017 M NaCl it was found at −0.530 V vs. SCE while in 0.170 M NaCl it is observed at −0.636 V vs. SCE. In Fig. 5(b) the breakdown potential, E_{br}, is plotted as a function of the logarithm of the chloride concentration to give a linear relationship, as illustrated in Eq. (8). The slope value of −0.108 ± 0.012 V shows the influence of chloride concentration on the dissolution behavior of the alloy. Similar experiments carried out with pure Al gave a much higher dependence on chloride concentration with a gradient of −0.204 V. The surface morphology following dissolution is shown in the inset in Fig. 5(a), where clusters of pits were evident and appear to merge to give a corroded area of about 100 μm in diameter.

$$E_{br} = -0.712 - 0.108 \log[Cl^-] \tag{8}$$

In the presence of phosphates, the polarisation behavior and the surface morphology are altered, as illustrated in Fig. 6. This is consistent with the corrosion inhibition properties of phosphates [30]. There is a 50 mV shift in the E_{corr} value to more positive potentials and a reduction in j_{corr} from 1.09×10^{-6} A cm^{-2} to 7.13×10^{-7} A cm^{-2} on the addition of phosphates. A hysteresis loop exists and is clearly evident as the potential is reversed and cycled to lower values. This

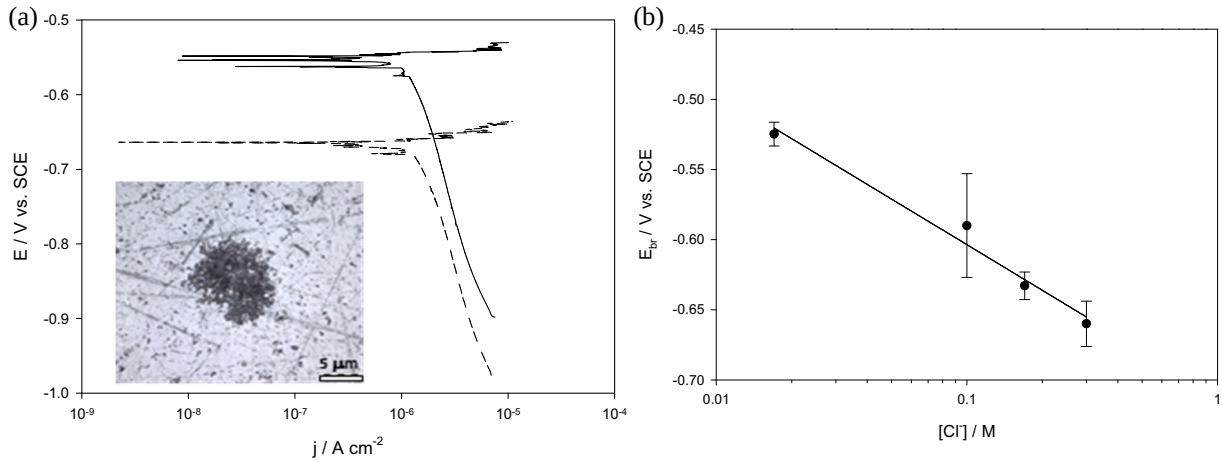

Fig. 5. (a) Potentiodynamic polarisation curves for Al – Mg in —— 0.017 M and – – – 0.170 M NaCl solutions at a pH of 5.0, recorded at 1 mV s^{-1}, micrograph shown in inset, (b) breakdown potential, E_{br}, as a function of the logarithm of the chloride concentration (n = 4).

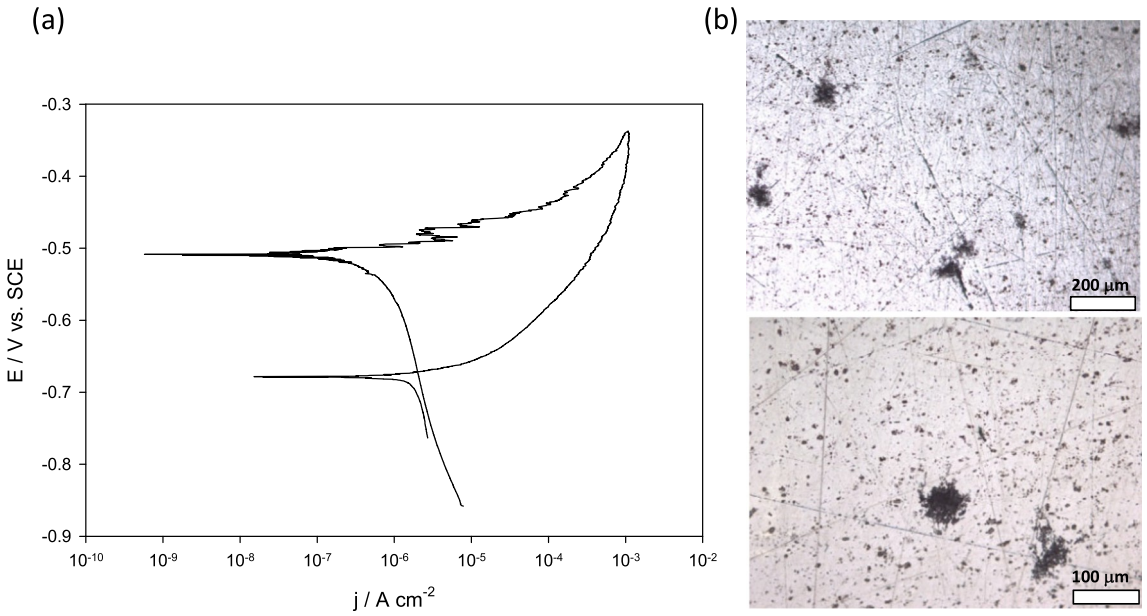

Fig. 6. (a) Cyclic polarisation curve recorded at 1 mV s^{-1} for Al−Mg in 0.017 M NaCl and 8.12 × 10^{-4} M phosphate, (b) micrographs recorded at the end of the cyclic potentiodynamic polarisation scan.

indicates that while the phosphates inhibit the initiation and propagation of the pits, once the pits are activated they continue to develop and are difficult to repassivate. The micrographs presented in Fig. 6(b) show that localised corrosion occurs, however the size of the pit clusters is somewhat smaller, with diameters reaching 80 µm. In addition to the circular−like clusters seen in the chloride solutions, some irregular−shaped clusters are evident in the presence of phosphates. These data clearly show that while phosphates are corrosion inhibitors, the Al−Mg alloy can be activated to induce dissolution in the presence of phosphates and the variations in chloride concentration have less influence on the dissolution of Al−Mg compared to pure Al. This is consistent with the data presented in Fig. 1 where the removal of phosphate is efficient in a relatively low (4.2 mM) concentration of chloride.

Electrochemical impedance data, shown as a complex plane impedance plot, are presented in Fig. 7, where the impedance is compared for pure Al and Al−Mg. The symbols show the experimental data, while the dotted traces represent the simulated data. The data were recorded

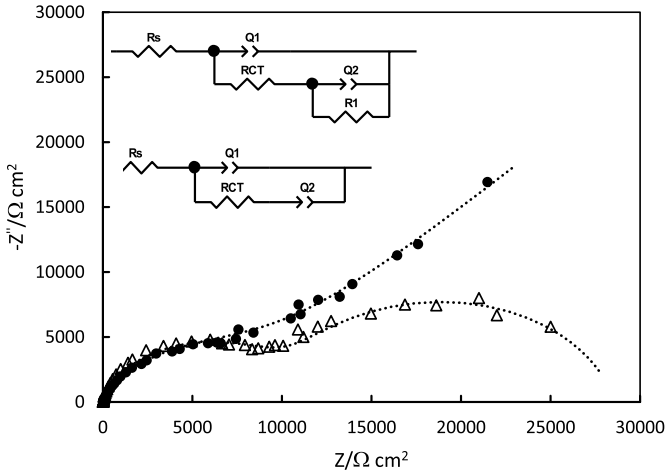

Fig. 7. Impedance data with equivalent circuits recorded for ● pure Al and Δ Al−Mg in 0.17 M NaCl under open−circuit conditions, dotted traces represent the simulated data generated using the equivalent circuits.

at the open−circuit potentials, −0.88 V vs SCE for Al−Mg and −0.72 V vs SCE for pure Al in a 0.17 M NaCl solution following a 2−h period in order to achieve steady−state conditions. The open−circuit potential adopted by the Al−Mg alloy following a 2−h immersion period is lower than the E_{corr} value evident in Fig. 5 and this is due to the fact that the electrode is polarised from below the E_{corr} value at a relatively slow rate in Fig. 5. The equivalent circuits employed in fitting the data are shown in the figure, where the two−time constant model was used to represent the Al−Mg alloy. In these circuits, R_s corresponds to the solution resistance, Q_1 represents a constant phase element, R_{CT} denotes the charge−transfer resistance and the additional R_1/Q_2 couple was used to represent the formation of a corrosion layer at the Al−Mg. The circuit parameters are summarised in Table 3. It is evident from a comparison of the figure and the data summarised in the table, that the impedance is different for the two systems. The pure Al is characterised by a R_{CT}/Q_1 couple representing a distorted capacitance and a charge−transfer resistance and an additional constant phase element, Q_2, which corresponds to a diffusional element (n = 0.52). This is consistent with the formation of a passive layer. On the other hand, the Al−Mg alloy has a higher charge−transfer resistance and this is possibility connected to the build−up of corrosion products. The additional R_1/Q_2 couple (n = 0.87 for Q) is consistent with the formation of corrosion products at the surface as a result of the dissolution of the alloy. These polarisation and impedance data show that Al−Mg is prone to dissolution, in the presence of chloride anions, and this is consistent with the good removal of phosphates, Figs. 1 and 2.

3.3. Adsorption processes

It is reasonable to assume that the adsorption processes associated with electrocoagulation are rapid and at the end of the electrocoagulation process equilibrium is achieved. Consequently, the

Table 3
Summary of impedance data recorded for Al−Mg and Al.

System	R_{CT}/kΩ cm^2	Q_1/Ω^{-1} cm^{-2} s^{n1}	n_1	R_1/kΩ cm^2
Al−Mg	10.6	3.1 × 10^{-5}	0.85	16.2
Al	0.97	1.9 × 10^{-5}	0.81	–

concentration of phosphate at equilibrium, P_e, can be taken as the final concentration of phosphate in solution, P_t. To support this assumption, the residual concentration of phosphate in solution was measured as a function of time immediately after stopping the coagulant dosing. It was observed that equilibrium was achieved in the first 2 min as there was no further change in the residual concentration of phosphate after this interval. However, the concentration of phosphate was measured after 15 min to ensure equilibrium. The adsorption capacity was obtained using a mass equilibrium equation which is expressed Eq. (9), were, q_e is the amount of phosphate adsorbed at equilibrium per unit mass of adsorbent, P_o and P_e are the initial and the equilibrium concentrations of phosphate, respectively, V is the volume of the solution, and M is the amount of adsorbent.

$$q_e = \frac{(P_o - P_e)V}{m} \tag{9}$$

The electrogenerated adsorbent may comprise $Al(OH)_3$ as well as other hydrolysis products of aluminium. Consequently, the amount of adsorbent generated, m, is difficult to measure and instead was considered as the amount of Al^{3+} ions generated by electrodissolution of the Al−Mg electrode, m_{Al}. The total mass was calculated using Faraday's law, Eq. (10), where m is the mass, J is the current, t is the time, EW is the gram equivalent weight of the material and F is Faraday's constant. The evaluation of m_{Al} was achieved using Eq. (11), where W is the atomic weight, f is the mass fraction, and Z is the valence of the elements present in the alloy [31].

$$m = \frac{JtEW}{F} = \frac{JtW}{FZ} \tag{10}$$

$$m = m_{Al} + m_{Mg} = \frac{Jt}{F}\left(\frac{W_{Al}}{Z_{Al}}f_{Al} + \frac{W_{Mg}}{Z_{Mg}}f_{Mg}\right) \tag{11}$$

Two models were used, the Langmuir and Freundlich models. The Langmuir equation, Eq. (12), where q_m is the maximum sorption capacity and k_L represents the affinity of the binding sites, is based on monolayer adsorption without interaction between the adsorbed molecules. On the other hand, the Freundlich model, Eq. (13), proposes multilayer adsorption with a heterogeneous energetic distribution of active sites accompanied by interactions between adsorbed species. In this analysis, K_f and n are associated with the adsorption capacity.

$$q_e = \frac{q_m k_L P_e}{1 + k_L P_e} \tag{12}$$

$$q_e = k_F P_e^{1/n} \tag{13}$$

The experiments were carried out by varying the initial concentration of phosphate from 2 to 150 mg L^{-1} in solutions containing 4.2 mM NaCl at an initial pH of 5.0 and at a temperature of 25.0 ± 0.5 °C. Each experiment was performed in triplicate. Fig. 7 shows the amount of phosphate adsorbed at equilibrium per unit mass of Al^{3+} ions, q_e, as a function of the equilibrium concentration of phosphate, P_e. The non−linear regression plots for the Langmuir and the Freundlich models are displayed in Fig. 8 with the corresponding experimental plot. The goodness of fit of the two models was tested using the adjusted R^2 value and the data are summarised in Table 4. Clearly, the Freundlich model gives a better fit and adsorption is favoured with a k_F value of 146 mg g^{-1} and n is higher than 1.0. This suggests that the phosphates are removed through an adsorption process. The Freundlich equation, although empirical, implies that the affinity for the adsorption sites decreases exponentially with increasing saturation. This assumption is more realistic than the constant binding energy inherent in the Langmuir equation. These data are consistent with the variations in pH and the speciation diagrams of hydrolysis products, Figs. 2 and 3, where adsorption is facilitated by the cationic hydroxy aluminium species and anionic phosphates.

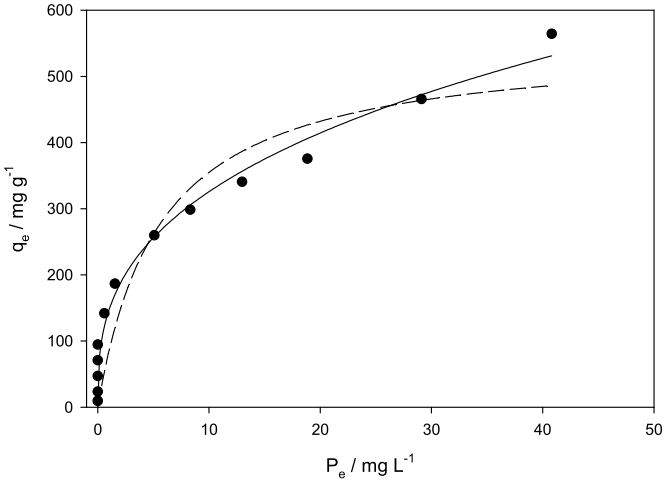

Fig. 8. Adsorption plots with ● Experimental data —— Freundlich isotherm, and − − − Langmuir isotherm fitting at 25.0 ± 0.5 °C.

Table 4
Langmuir and Freundlich model constants and adjusted R^2 values.

Langmuir model			Freundlich model		
k_L/L mg^{-1}	q_m/mg g^{-1}	Adjusted R^2	k_F/mg g^{-1}	n	Adjusted R^2
0.18 ± 0.08	552 ± 69	0.883	146 ± 22	2.9 ± 0.1	0.943

3.4. Removal of phosphates from real water samples

Given the positive results obtained for the removal of phosphates in the presence of low chloride concentrations, the Al−Mg electrode was used as an anode material to treat real wastewater samples that were obtained from two wastewater facilities and these are labelled as Sample A and B. The samples were collected at the primary settlement areas and their physico-chemical characteristics, such as the pH, the concentration of chloride ions, the conductivity and the concentration of phosphate ions, are presented in Table 5. The samples were used in electrocoagulation tests without any pre-treatment but 10 mg L^{-1} of phosphate was added to Sample A, as the concentration of phosphate was very low. Fig. 9 shows the efficiency of removal plotted as a function of the electrocoagulation period for both samples. It is clear that at the end of 15 min the phosphate ions are completely removed from both samples. For comparison purposes, similar data are shown for pure Al using Sample A. Again, good removal is achieved, however, the efficiency is lower at the earlier times when compared to the Al−Mg alloy.

4. Conclusions

It is evident from this study that aluminium alloyed with magnesium to give Al−Mg provides efficient removal of phosphates at different concentrations of chloride, pH and also in real water samples. The removal of phosphates is achieved within 15 min in real water samples. Al−Mg alloys are used in a variety of engineering applications and like pure aluminium, they are light weight alloys. Their efficiency in removing phosphates appears to be related to the ease of dissolution

Table 5
Physico−chemical characteristics for the real samples A and B.

Sample	pH	Cl^-/mM	κ/mS cm^{-1}	P/mg L^{-1}
A	6.8	0.71 ± 0.03	0.32	1.1
B	7.4	4.74 ± 0.04	1.00	4.6

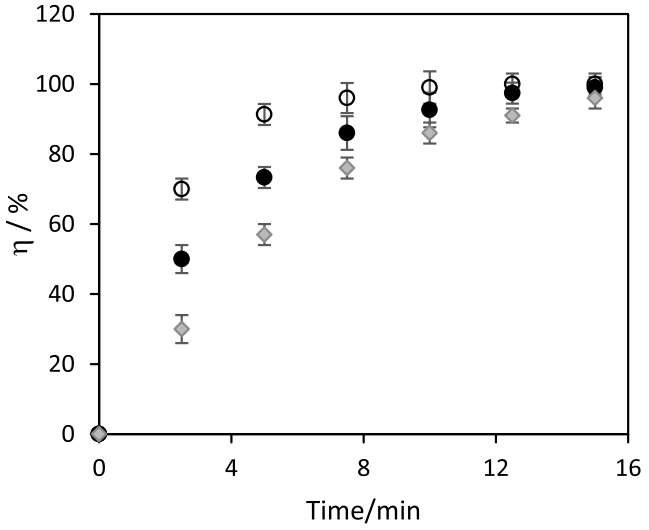

Fig. 9. The removal efficiency plotted as a function of the electrocoagulation time for real water samples, ● Sample A and ○ Sample B with Al – Mg anodes and ♦ Sample A with pure Al (n = 3).

of the alloy which was evident using polarisation, cyclic polarisation and electrochemical impedance spectroscopy. Furthermore, dissolution of the Al – Mg alloy appears to be more general – like compared to the deep pitting attack that is seen with pure aluminium. Al—Mg is less susceptible to passivation compared with pure Al, making this alloy suitable as an anode in electrocoagulation. The simple two electrode system used in this study can be easily scaled up to give multiple and alternating cathodes with Al – Mg anodes that facilitate the flow of water through the unit, making it suitable for small-scale water treatment facilities. Furthermore, it is apparent that potentiodynamic and cyclic polarisation curves coupled with Tafel analysis and electrochemical impedance spectroscopy are convenient and simple techniques that can be used to provide information on the probable performance of an anode in electrocoagulation studies.

Acknowledgements

The authors would like to acknowledge funding from the Irish Research Council, EMBARK initiative.

References

[1] E. Valsami-Jones, Phosphorus in Environmental Technologies: Principles and Applications, IWA Publishing, 2004.
[2] P.W.W. Kirk, R. Perry, M. Hunter, J.N. Lester, P.J. Matthews, Phosphorus removal by pre – precipitation of sewage: metal removal, sludge characteristics and treatment efficiency, Environ. Technol. Lett. 9 (1988) 171–180.
[3] E. Diamadopoulos, A. Benedek, Aluminum hydrolysis effects on phosphorus removal from wastewaters, J. Water Pollut. Control Fed. 56 (1984) 1165–1172.
[4] E. Lacasa, P. Canizares, C. Saez, F.J. Fernandez, M.A. Rodrigo, Electrochemical phosphates removal using iron and aluminium alloys, Chem. Eng. J. 172 (2011) 137–143.
[5] M.R. Awual, A. Jyo, S.A. El-Safty, M. Tamada, N. Seko, A weak – base fibrous anion exchanger effective for rapid phosphate removal from water, J. Hazard. Mater. 188 (2011) 164–171.
[6] L. Delgadillo-Velasco, V. Hernandez-Montoya, N.A. Rangel-Vazquez, F.J. Cervantes, M.A. Montes-Moran, M. del R. Moreno-Virgen, Screening of commercial sorbents for the removal of phosphates from water and modeling by molecular simulation, J Molecular Liquids 262 (2018) 443–450.
[7] G. Sharma, J. Choi, H.K. Shon, S. Phuntsho, Solar – powered electrocoagulation system for water and wastewater treatment, Desalin. Water Treat. 32 (2011) 381–388.
[8] S. Garcia-Segura, M.M.S.G. Eiband, J. Vieira de Melo, C.A. Martinez-Huitle, Electrocoagulation and advance electrocoagulation processes: a general review about the fundamentals, emerging applications and its association with other technologies, J. Electroanal. Chem. 801 (2017) 267–299.
[9] A.S. Naje, S. Chelliapan, Z. Zakaria, M.A. Ajeel, P.A. Alaba, A review of electrocoagulation technology for the treatment of textile wastewater, Rev. Chem. Eng. 33 (2017) 263–– 292.
[10] M. Elazzouzi, Kh. Haboubi, M.S. Elyoubi, Electrocoagulation flocculation as a low – cost process for pollutants removal from urban wastewater, Chem. Eng. Research Design 117 (2017) 614–626.
[11] S. Irdemez, N. Demircioglu, Y.S. Yildiz, Z. Bingul, The effects of current density and phosphate concentration on phosphate removal from wastewater by electrocoagulation using aluminum and iron plate electrodes, Sep. Purif. Technol. 52 (2006) 218–223.
[12] K.S. Hashim, R. Al Khaddar, N. Jasim, A. Shaw, D. Phipps, P. Kot, M.O. Pedrola, A.W. Alattabi, M. Abdulredha, R. Alawsh, Electrocoagulation as a green technology for phosphate removal from river water, Sep. Purif. Technol. 210 (2019) 135–144.
[13] N. Bektas, H. Akbulut, H. Inan, A. Dimoglo, Removal of phosphate from aqueous solutions by electrocoagulation, J. Hazard. Mater. 106 (2004) 101–105.
[14] S. Vasudevan, G. Sozhan, S. Ravichandran, J. Jayaraj, J. Lakshmi, S.M. Sheela, Studies on the removal of phosphate from drinking water by electrocoagulation process, Ind. Eng. Chem. Res. 47 (2008) 2018–2023.
[15] A. Dura, C.B. Breslin, Electrocoagulation using aluminium anodes activated with Mg, In and Zn alloying elements, J. Hazard. Mater. 366 (2019) 39–45.
[16] K. Mansouri, K. Ibrik, N. Bensalah, A. Abdel-Wahab, Anodic dissolution of pure aluminium during electrocoagulation process: influence of supporting electrolyte, initial pH, and current density, Ind. Eng. Chem. Res. 50 (2011) 13362–13372.
[17] P.K. Holt, G.W. Barton, C.A. Mitchell, The future for electrocoagulation as a localized water treatment technology, Chemosphere 59 (2005) 355–367.
[18] M. Kobya, O.T. Can, M. Bayramoglu, Treatment of textile wastewaters by electrocoagulation using iron and aluminum electrodes, J. Hazard. Mater. 100 (2003) 163–178.
[19] G. Gonzales, E. Touraud, S. Spinelli, O. Thomas, Organic constituents, in: O. Thomas, C. Burgess (Eds.), UV–Visible Spectrophotometry of Water and Wastewater, Elsevier, 2007.
[20] Z.V.P. Murthy, S. Parmar, Removal of strontium by electrocoagulation using stainless steel and aluminum electrodes, Desalination 282 (2011) 63–67.
[21] F. Akbal, S. Camci, Treatment of metal plating wastewater by electrocoagulation, Environ. Prog. Sustain. Energy 31 (2012) 340–350.
[22] N. Bektas, H. Akbulut, H. Inan, A. Dimoglo, Removal of phosphate from aqueous solutions by electrocoagulation, J. Hazard. Mater. 106 (2004) 101–105.
[23] S. Vasudevan, J. Lakshmi, J. Jayaraj, G. Sozhan, Remediation of phosphate – -contaminated water by electrocoagulation with aluminum, aluminum alloy and mild steel anodes, J. Hazard. Mater. 164 (2009) 1480–1486.
[24] S. Irdemez, Y.S. Yildiz, V. Tosunoglu, Optimization of phosphate removal from wastewater by electrocoagulation with aluminum plate electrodes, Sep. Purif. Technol. 52 (2006) 394–401.
[25] G. Eriksson, An algorithm for the computation of aqueous multicomponent, multiphase equilibriums, Anal. Chim. Acta 112 (1979) 375–383.
[26] I. Kabdasli, A. Keles, T. Oelmez-Hanci, O. Tuenay, I. Arslan-Alaton, Treatment of phthalic acid esters by electrocoagulation with stainless steel electrodes using dimethyl phthalate as a model compound, J. Hazard. Mater. 171 (2009) 932–940.
[27] G. Mouedhen, M. Feki, M.D.P. Wery, H.F. Ayedi, Behavior of aluminum electrodes in electrocoagulation process, J. Hazard. Mater. 150 (2008) 124–135.
[28] G.H. Chen, Electrochemical technologies in wastewater treatment, Sep. Purif. Technol. 38 (2004) 11–41.
[29] P. Canizares, F. Martinez, C. Jimenez, J. Lobato, M.A. Rodrigo, Coagulation and electrocoagulation of wastes polluted with dyes, Environ. Sci. Technol. 40 (2006) 6418–6424.
[30] K. – .H. Na, S.I. Pyun, Effects of sulphate, nitrate and phosphate on pit initiation of pure aluminium in HCl – based solution, Corros. Sci. 49 (2007) 2663–2675.
[31] C. Cuevas-Arteaga, J. Porcayo-Calderon, Electrochemical noise analysis in the frequency domain and determination of corrosion rates for SS – 304 stainless steel, Mater. Sci. Eng. A 435 (2006) 439–446.